Supplementary Information

Polydopamine-Gated Biodegradable Cascade Nanoreactor for pH-Triggered and Photothermal-Enhanced Tumor-Specific Nanocatalytic Therapy

Fanghui Chen[a], Peijing An[a], Ling Liu[b], Zhiguo Gao[a], Yaojia Li[a], Yuchen Zhang[a], Baiwang Sun[a,c,*], Jiancheng Zhou[a,*]

a: School of Chemistry and Chemical Engineering, Southeast University, Nanjing 211189, China

b: Department of Infectious Diseases, Hospital of Integrated Traditional Chinese and Western Medicine Affiliated with Nanjing University of Chinese Medicine, Nanjing 210028, China

c: Jiangsu Province Hi-Tech Key Laboratory for Biomedical Research, Southeast University, Nanjing 211189, China

Corresponding authors, E-mail addresses: chmsunbw@seu.edu.cn (Baiwang Sun); jczhou@seu.edu.cn (Jiancheng Zhou)

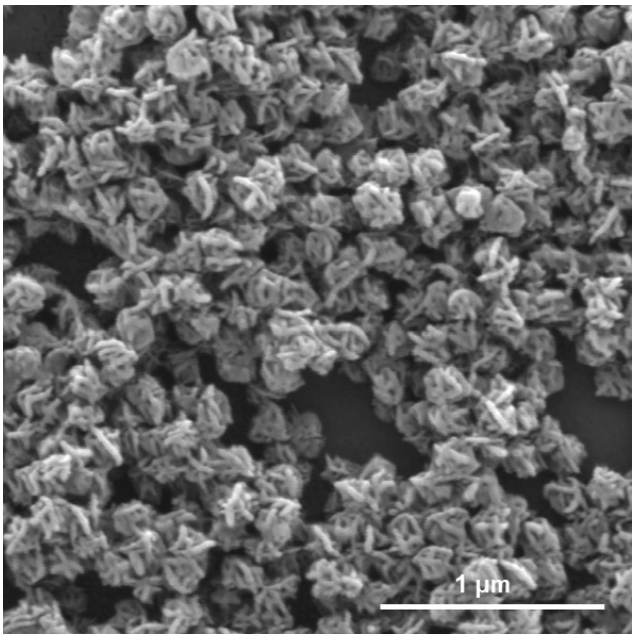

Fig. S1. SEM image of the as-prepared $hMnO_2$ nanostructures.

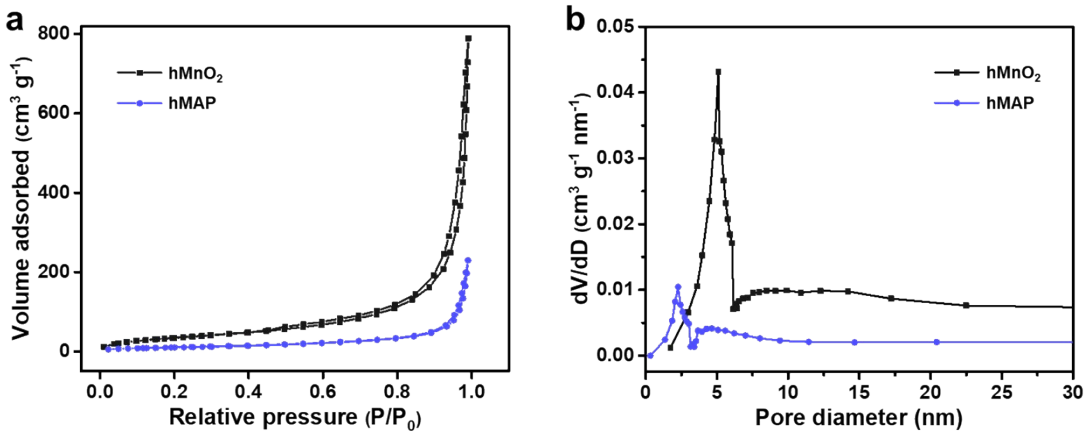

Fig. S2. (a) N_2 adsorption-desorption isotherm and (b) corresponding pore-size distribution of $hMnO_2$ and hMAP.

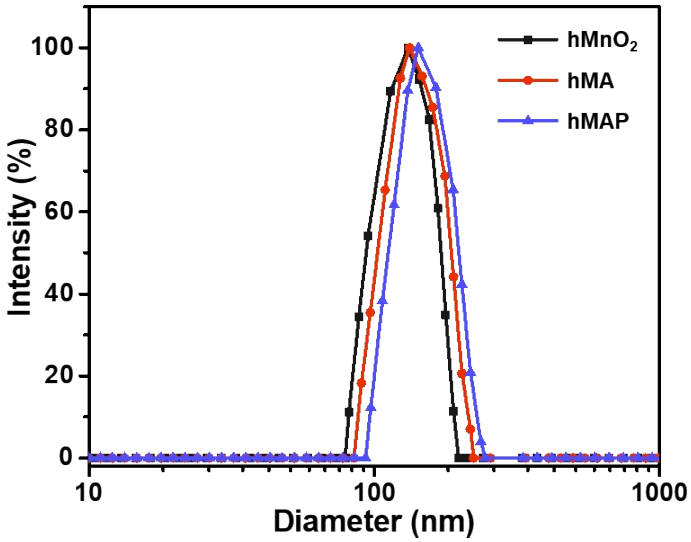

Fig. S3. Hydrodynamic diameter distribution of $hMnO_2$, hMA and hMAP measured by DLS.

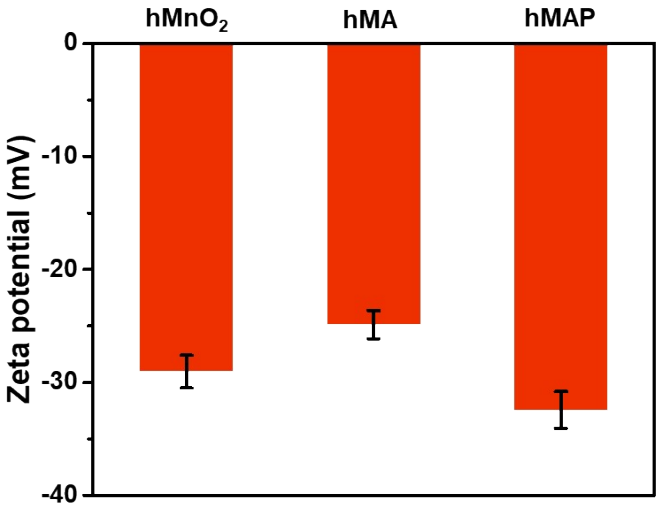

Fig. S4. The zeta potential of $hMnO_2$, hMA and hMAP.

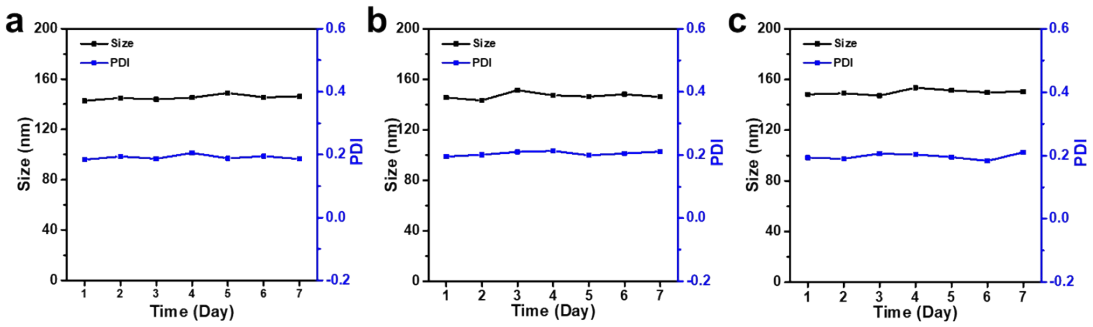

Fig. S5. The hydrodynamic size and PDI changes of hMAP dispersed in (a) water, (b) PBS, and (c) RPMI-1640 medium containing 10% FBS for 7 days.

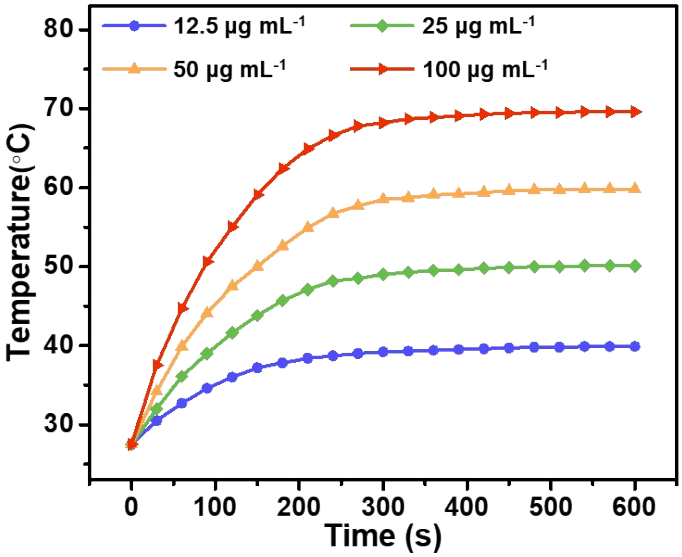

Fig. S6. Temperature variation curves of hMAP at different $hMnO_2$ concentrations (12.5, 25, 50 and 100 μg mL^{-1}) with 808 nm laser irradiation at 1.5 W cm^{-2} for 600s.

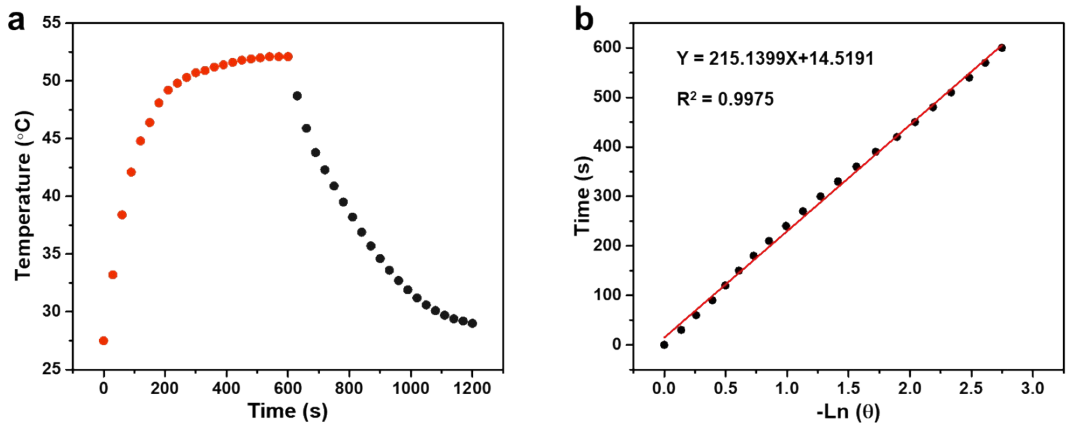

Fig. S7. (a) Heating and cooling curves of hMAP aqueous solution (1.0 mL, 100 μg/mL) under irradiation of 808 nm laser (1.0 W/cm^2). (b) Plot of cooling time versus negative natural logarithm of the temperature driving force.

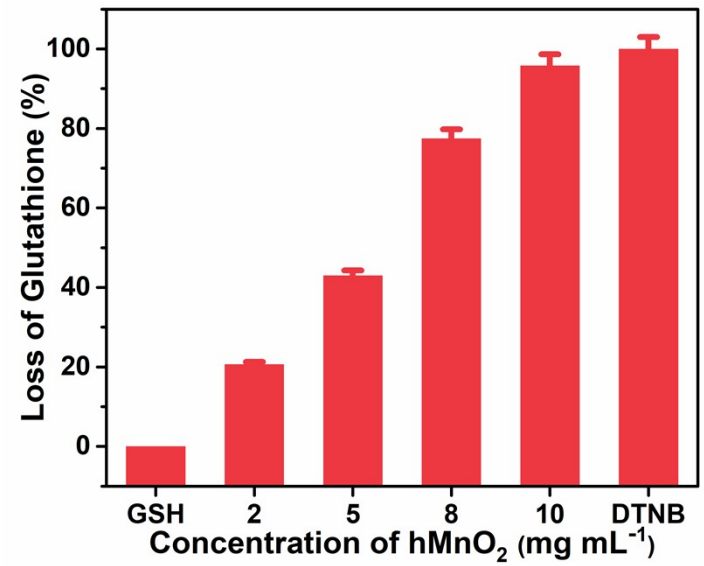

Fig. S8. The degradation percent of GSH by different concentrations of $hMnO_2$, [DTNB] = 0.3 mM, [GSH] = 0.5 mM.

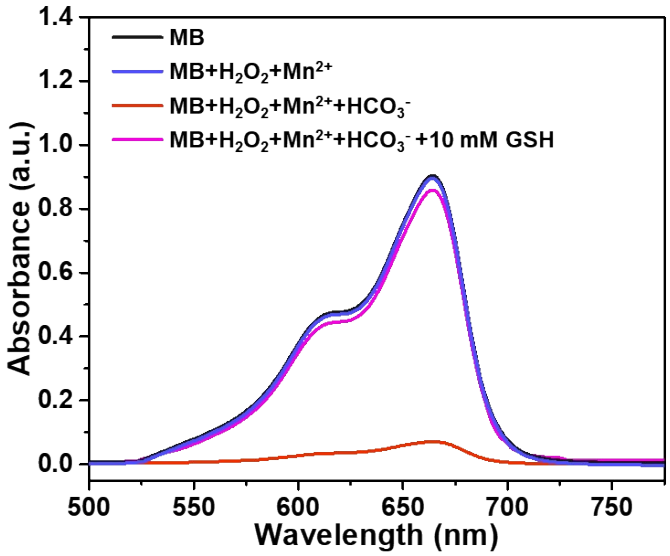

Fig. S9. UV-vis absorption spectra of MB degradation in different solutions ([Mn] = 0.5 mM, [H_2O_2] = 8 mM, [$NaHCO_3$/5% CO_2] = 25 mM, [MB] = 6 μg mL^{-1}).

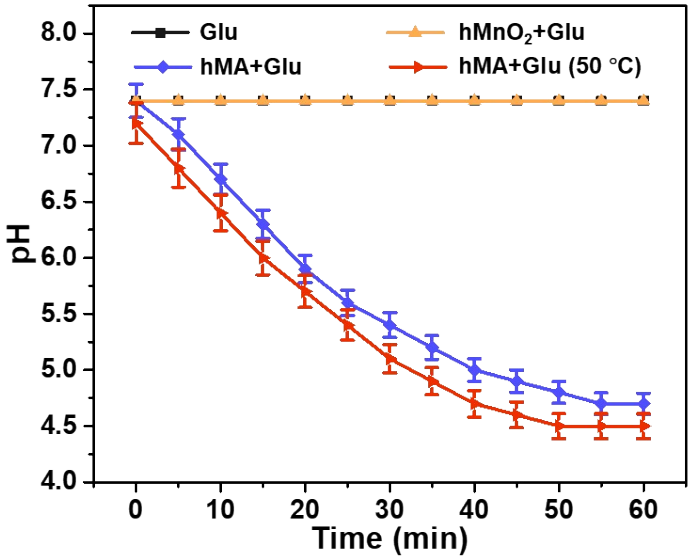

Fig. S10. Time-dependent variations of pH values after incubation with $hMnO_2$ or hMA (RT or 50 °C) in the presence of glucose (2 mM).

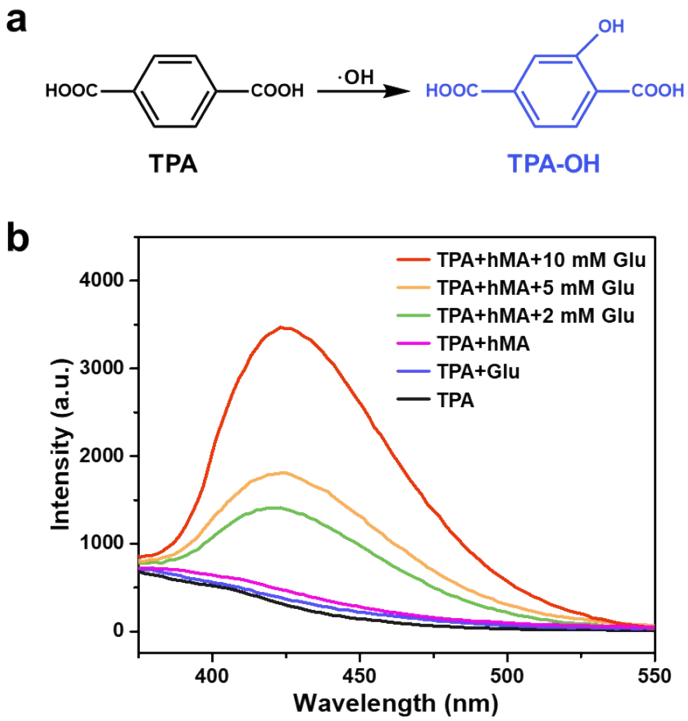

Fig. S11. (a) Nonfluorescent compound terephthalic acid (TPA) reacts with hydroxyl radical (·OH) to form stable fluorescent 2-hydroxy-terephalic acid (TPA-OH). (b) Fluorescence spectra of TPA-OH induced by hMA with different concentrations of glucose.

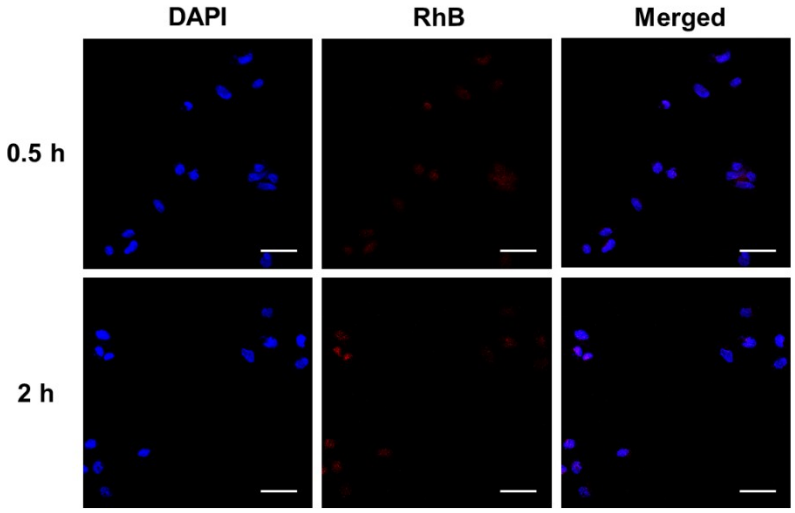

Fig. S12. CLSM images of LO2 cells incubated with RhB-labeled hMAP for 0.5 h and 2 h (scale bars: 50 μm).

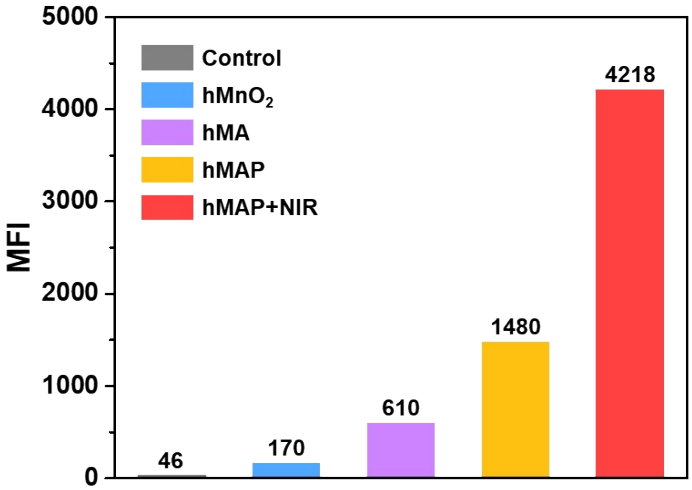

Fig. S13. The mean fluorescence intensity of ROS generation in MCF-7 cells after various treatments.

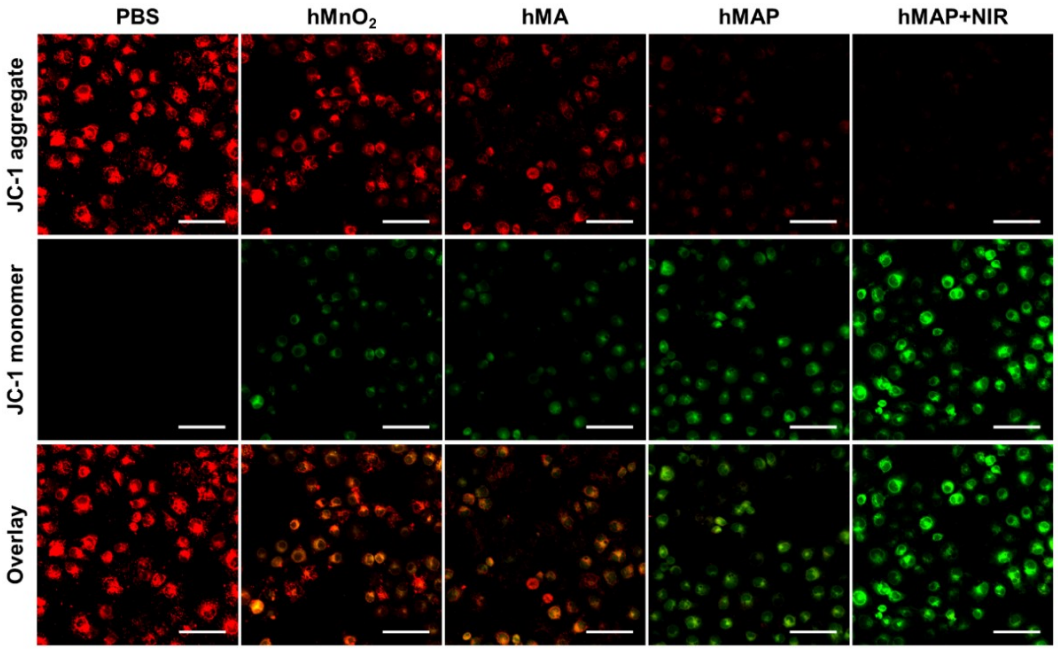

Fig. S14. JC-1 staining of MCF-7 cells after different treatments (scale bars: 100 μm).

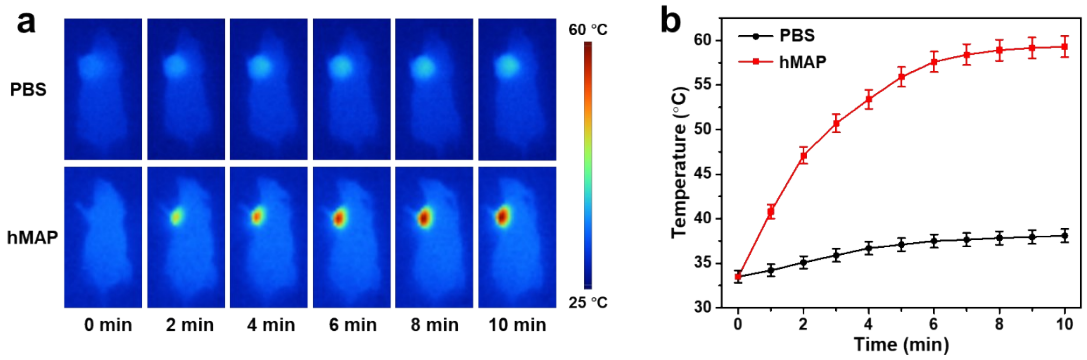

Fig. S15. (a) Thermal images and (b) the corresponding heating curves of MCF-7 tumor-bearing mice during 808 nm laser irradiation (1 W cm^{-2}, 10 min) at 12 h post-injection of PBS or hMAP.

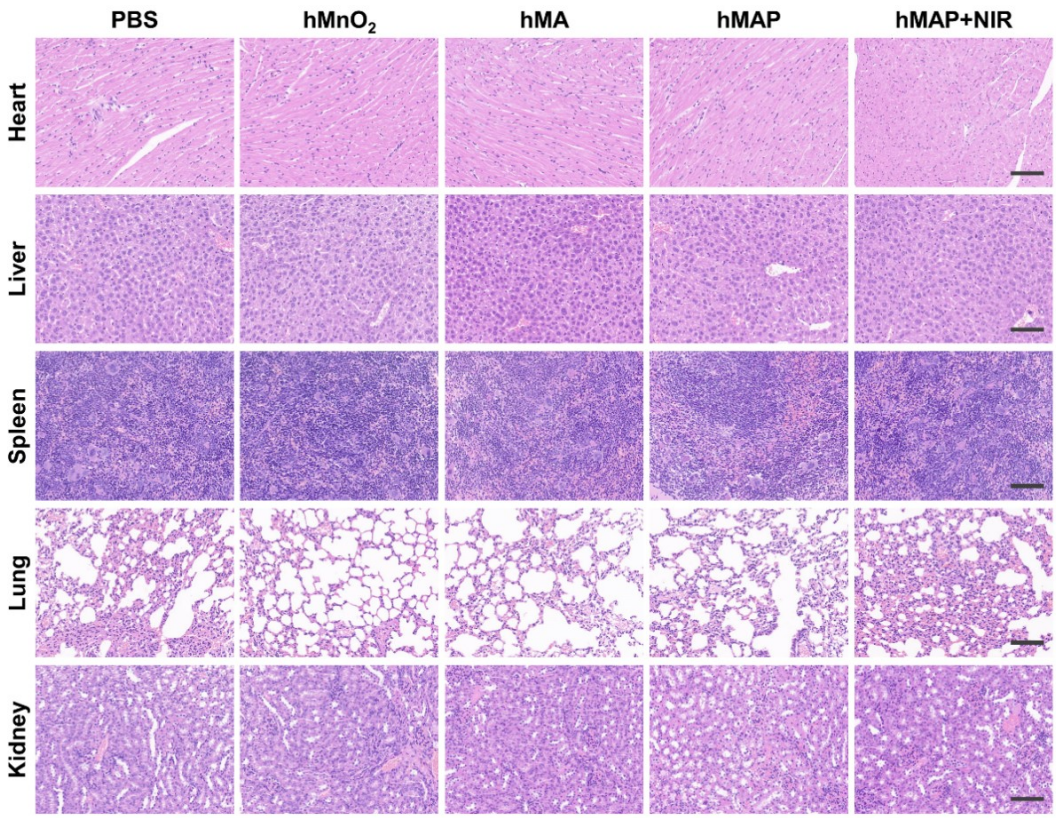

Fig. S16. H&E staining images of major organs on MCF-7 tumor-bearing mice after different treatments. Scale bar: 100 μm.